UNIVERSITY *of York*

This is a repository copy of *Inverse odd-even staggering in nuclear charge radii and possible octupole collectivity in ^{217,218,219}At revealed by in-source laser spectroscopy*.

Version: Published Version

Inverse odd-even staggering in nuclear charge radii and possible octupole collectivity in ^{217,218,219}At revealed by in-source laser spectroscopy

A. E. Barzakh,[1,*] J. G. Cubiss,[2] A. N. Andreyev,[2,3,4] M. D. Seliverstov,[1,2] B. Andel,[5] S. Antalic,[5] P. Ascher,[6] D. Atanasov,[6] D. Beck,[7] J. Bieroń,[8] K. Blaum,[6] Ch. Borgmann,[6] M. Breitenfeldt,[9] L. Capponi,[10] T. E. Cocolios,[4,11] T. Day Goodacre,[4,11] X. Derkx,[10,12] H. De Witte,[9] J. Elseviers,[9] D. V. Fedorov,[1] V. N. Fedosseev,[4] S. Fritzsche,[13,14] L. P. Gaffney,[9] S. George,[6] L. Ghys,[9,15] F. P. Heßberger,[16,17] M. Huyse,[9] N. Imai,[4,18] Z. Kalaninová,[5,19] D. Kisler,[6] U. Köster,[20] M. Kowalska,[4] S. Kreim,[6,4] J. F. W. Lane,[10] V. Liberati,[10] D. Lunney,[21] K. M. Lynch,[4,11] V. Manea,[4,21] B. A. Marsh,[4] S. Mitsuoka,[3] P. L. Molkanov,[1] Y. Nagame,[3] D. Neidherr,[7] K. Nishio,[3] S. Ota,[3] D. Pauwels,[15] L. Popescu,[15] D. Radulov,[9] E. Rapisarda,[4] J. P. Revill,[22] M. Rosenbusch,[23,24] R. E. Rossel,[4,25] S. Rothe,[4,25] K. Sandhu,[10] L. Schweikhard,[23] S. Sels,[9] V. L. Truesdale,[2] C. Van Beveren,[9] P. Van den Bergh,[9] P. Van Duppen,[9] Y. Wakabayashi,[3] K. D. A. Wendt,[25] F. Wienholtz,[23,4] B. W. Whitmore,[2] G. L. Wilson,[2] R. N. Wolf,[6,†] and K. Zuber[26]

[1]*Petersburg Nuclear Physics Institute, NRC Kurchatov Institute, 188300 Gatchina, Russia*
[2]*Department of Physics, University of York, York, YO10 5DD, United Kingdom*
[3]*Advanced Science Research Center, Japan Atomic Energy Agency, Tokai-Mura, Naka-gun, Ibaraki 319–1195, Japan*
[4]*CERN, CH-1211 Geneva 23, Switzerland*
[5]*Department of Nuclear Physics and Biophysics, Comenius University in Bratislava, 84248 Bratislava, Slovakia*
[6]*Max-Planck-Institut für Kernphysik, 69117 Heidelberg, Germany*
[7]*GSI Helmholtzzentrum für Schwerionenforschung GmbH, 64291 Darmstadt, Germany*
[8]*Instytut Fizyki imienia Mariana Smoluchowskiego, Uniwersytet Jagielloński, ul. prof. Stanisława Łojasiewicza 11, Kraków, Poland*
[9]*KU Leuven, Instituut voor Kern- en Stralingsfysica, B-3001 Leuven, Belgium*
[10]*School of Engineering, University of the West of Scotland, Paisley PA1 2BE, United Kingdom*
[11]*School of Physics and Astronomy, The University of Manchester, Manchester M13 9PL, United Kingdom*
[12]*LPC, ENSICAEN, Université de Caen Basse Normandie, CNRS/IN2P3-ENSI, Caen F-14050, France*
[13]*Helmholtz-Institut Jena, Fröbelstieg 3, D-07743 Jena, Germany*
[14]*Theoretisch-Physikalisches Institut, Friedrich-Schiller-Universität Jena, Max-Wien-Platz 1, D-07743 Jena, Germany*
[15]*Belgian Nuclear Research Center SCKCEN, Boeretang 200, B-2400 Mol, Belgium*
[16]*Gesellschaft für Schwerionenforschung, Planckstrasse 1, D-64291 Darmstadt, Germany*
[17]*Helmholtz Institut Mainz, 55099 Mainz, Germany*
[18]*High Energy Accelerator Research Organisation (KEK), Oho 1-1, Tsukuba, Ibaraki 305–0801, Japan*
[19]*Laboratory of Nuclear Problems, JINR, 141980 Dubna, Russia*
[20]*Institut Laue Langevin, 71 avenue des Martyrs, F-38042 Grenoble Cedex 9, France*
[21]*CSNSM-IN2P3-CNRS, Université Paris-Sud, 91406 Orsay, France*
[22]*Oliver Lodge Laboratory, University of Liverpool, Liverpool, L69 7ZE, United Kingdom*
[23]*Universität Germany, Institut für Physik, 17487 Greifswald, Germany*
[24]*RIKEN Nishina Center for Accelerator-Based Science, Wako, 351-098 Saitama, Japan*
[25]*Institut für Physik, Johannes Gutenberg-Universität, D-55099 Mainz, Germany*
[26]*Technische Universität Dresden, 01069 Dresden, Germany*

Hyperfine-structure parameters and isotope shifts for the 795-nm atomic transitions in ^{217,218,219}At have been measured at CERN-ISOLDE, using the in-source resonance-ionization spectroscopy technique. Magnetic dipole and electric quadrupole moments, and changes in the nuclear mean-square charge radii, have been deduced. A large inverse odd-even staggering in radii, which may be associated with the presence of octupole collectivity, has been observed. Namely, the radius of the odd-odd isotope ^{218}At has been found to be larger than the average

---

*barzakh@mail.ru

†Present address: ARC Centre of Excellence for Engineered Quantum Systems, School of Physics, The University of Sydney, NSW 2006, Australia.

of its even-N neighbors, ^{217,219}At. The discrepancy between the additivity-rule prediction and experimental data for the magnetic moment of ^{218}At also supports the possible presence of octupole collectivity in the considered nuclei.

I. INTRODUCTION

The possible presence of octupole correlations has been conjectured for nuclei with the neutron and proton numbers N and Z in the $130 \leqslant N \leqslant 140, 86 \leqslant Z \leqslant 92$ region, where the Fermi surface lies between shell-model states with $\Delta j = \Delta l = 3$, where j and l are the total angular and orbital moments. For the considered region, it is the proton $f_{7/2}, i_{13/2}$ states and the neutron $g_{9/2}, j_{15/2}$ orbitals that satisfy these conditions. In such cases the nucleus can assume octupole deformation, corresponding to reflection asymmetry in the intrinsic frame, either dynamically (octupole vibrations) or by having a static shape (permanent octupole deformation) [1,2].

Experimentally, the signs of octupole deformation were found in a number of ways (see Refs. [1,2]), including α decay to low-lying negative-parity states in the even-even nuclei [3], Coulomb excitation [4], or from the comparison of experimental nuclear masses with models where reflection asymmetry is taken into account [5].

Another sign of octupole effects in this region is the occurrence of a so-called inverse odd-even staggering (inverse OES) in the charge radii of an isotopic chain. Throughout the nuclide chart, an OES in charge radii is systematically observed, whereby an odd-N isotope has a smaller charge radius than the average of its two even-N neighbors. However, an inversion of OES has been found in some regions of the nuclide chart, in particular, for the $N = 133-139$ francium and radium isotopes [6].

The correlation between octupole deformation and inverse OES was qualitatively described by Otten [6] and corroborated by the calculations of Leander and Sheline [7], as due to an increase in the mean-square octupole deformation ($\langle \beta_3^2 \rangle$) for odd-$N$ nuclei, relative to their even-N neighbors. The schematic calculations by Talmi [8] also imply a normal OES for even-multipole deformations and inverse OES for odd-multipole deformations.

However, one cannot consider inverse OES as a definite "fingerprint" of octupole collectivity, despite the strong correlation between these two phenomena. In particular, the inverse OES in several francium and radium isotopes could also be qualitatively reproduced in the framework of the extended Thomas-Fermi approach without invoking odd-order contributions to the deformation [9] (see also the discussion on the octupole deformation and inverse OES in europium and barium isotopes near $N = 88-90$ [10–14]).

Recently, new information on the borders of the inverse-OES region at $Z > 82$ was obtained via laser-spectroscopy investigations of $_{84}$Po [15], $_{87}$Fr [16], and $_{88}$Ra [17]. To better localize this region, in the present work we have undertaken isotope shift (IS) and hyperfine structure (hfs) investigations for ^{217,218,219}At. These nuclei lie in the vicinity of the presumed "octupole region" but so far have never been considered as reflection asymmetric.

The investigations presented in this paper are part of an experimental campaign at the ISOLDE facility (CERN) aimed at β-delayed fission, nuclear decay, and laser spectroscopy studies of the astatine isotopes. Partial results were reported in Refs. [18,19].

II. EXPERIMENTAL DETAILS

The present data came from the same experiment on the long chain of astatine isotopes at the ISOLDE facility, as described in detail in Ref. [19], which reported on charge radii and electromagnetic moments of $^{195-211}$At. Therefore, here we provide only a short description and refer the reader to Ref. [19] for full details on the experiment and data analysis.

The in-source laser spectroscopy technique [20,21] was used for IS and hfs measurements of astatine atoms. Radioactive astatine isotopes were produced in spallation reactions, induced by 1.4-GeV protons from the CERN PS Booster in a $50 \, \mathrm{g \, cm^{-2}}$ UC$_x$ target. The spallation products diffused through the target material as neutral atoms and effused into the hot cavity of the ion source. Laser beams were introduced into this cavity and performed selective ionization of the astatine isotopes of interest using a three-step ionization scheme [19]. The photoion current as a function of the laser frequency of the second excitation step ($46234 \, \mathrm{cm^{-1}} \to 58805 \, \mathrm{cm^{-1}}$; $795.2 \, \mathrm{nm}$) was measured by two methods. For the relatively short-lived isotopes, ^{217}At ($T_{1/2} = 32 \, \mathrm{ms}$) and ^{218}At ($T_{1/2} = 1.5 \, \mathrm{s}$), the α-decay rate was measured with the Windmill (WM) setup [22], whereas ion counting by the Multi-Reflection Time-of-Flight Mass Separator (MR-ToF MS) [23] was used for the longer lived ^{219}At ($T_{1/2} = 56 \, \mathrm{s}$).

A detailed account of hfs scanning with the Windmill setup and the MR-ToF MS device, and a description of the laser system can be found in Refs. [19,21,24]. Examples of experimental spectra are presented in Fig. 1.

III. RESULTS

The experimental spectra were fitted using the same method as described in detail in Ref. [19]. The fitting process requires the knowledge of a nuclear spin value, since the Doppler-limited resolution of the in-source laser-spectroscopy method does not allow an unambiguous determination of the spin in the astatine nuclei. Below we summarize available literature information on the possible spin and parity assignments based on the α- and β-decay properties of ^{217,218,219}At.

A. Nuclear spins assumed from the literature data

According to the nuclear data evaluation [25], the ground state of ^{217}At was assigned a spin (I) and parity (π) of $I^\pi = (9/2^-)$, based on the low hindrance factor [$HF = 1.16(4)$] of its α decay to the ground state of ^{213}Bi, which has a firmly
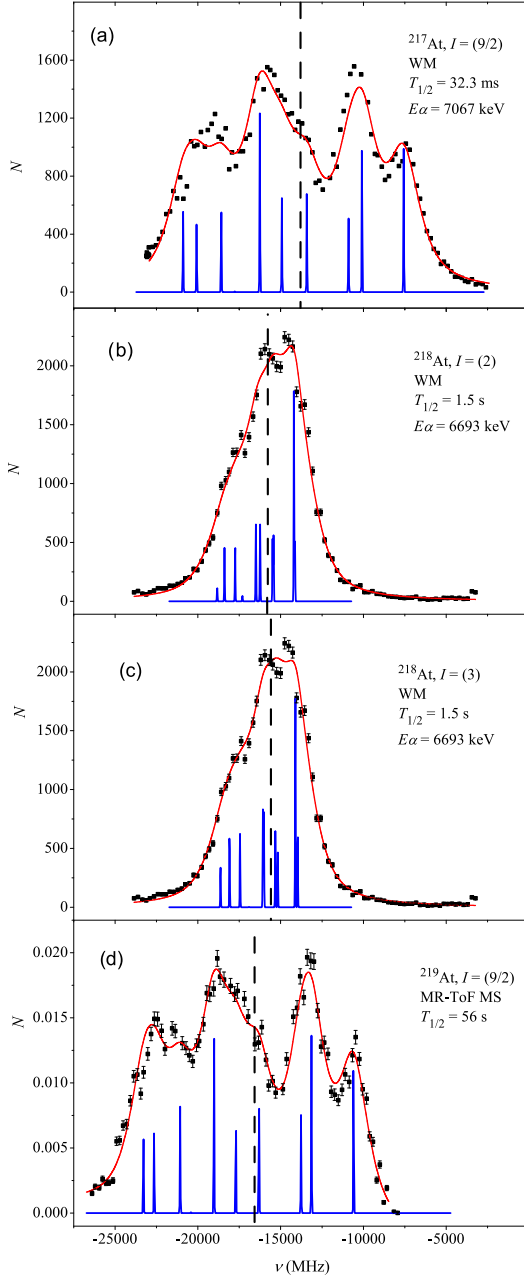
FIG. 1. Examples of experimental hfs spectra collected for the 795-nm transition. Frequency detuning is shown with respect to the centroid of ^{205}At hfs. The solid red lines represent a fit to the data. The blue lines indicate the calculated positions and relative intensities of the individual hyperfine components. The vertical dashed lines mark the hfs centroids. The isotope, the assumed nuclear spin, the half-life, the α lines used for the photo-ion current monitoring, and the device (windmill [WM] or multireflection time-of-flight mass separator [MR-ToF MS], see text for details) applied for the measurement are given in each panel. In the case of the WM, the number of recorded α counts of the indicated α line for each frequency step is displayed on the vertical axis. In the case of MR-ToF MS, the number of ions recorded in the MR-ToF MS system for every frequency setting, divided by the total number of counts in a full scan, is given on the vertical axis. In panels (b) and (c) fits of the experimental spectrum of ^{218}At with different possible spin assignments ($I = 2$ or 3) are shown.

TABLE I. Values of the isotope shifts, $\delta\nu_{A,205}$, and hyperfine splitting constants, a and b, for ^{217,218,219}At. For ^{218}At the results with the different possible spin assumptions (see Sec. III A) are presented.

Atomic number	I	$\delta\nu_{A,205}$(MHz)	a (MHz)	b (MHz)
217	(9/2)	$-13800(80)$	$-329(4)$	$-840(150)$
218	(2)	$-15810(130)$	$-239(17)$	$380(200)$
218	(3)	$-15590(130)$	$-167(16)$	$330(200)$
219	(9/2)	$-16580(120)$	$-311(4)$	$-700(150)$

established $I^{\pi}(^{213}\text{Bi}^g) = 9/2^-$. This spin and parity would correspond to a dominant $(\pi h_{9/2})^3$ configuration for ^{217}At.

Similarly, a value of $I^{\pi} = 9/2^-$ is suggested for the ^{219}At ground state, based on the low hindrance factor of the α decay of $^{219}\text{At}^g$ to $^{215}\text{Bi}^g$ ($HF = 1.1$) [26]. The ground state of ^{215}Bi is presumed to have $I^{\pi} = (9/2^-)$, in view of both the strong population of the $11/2^+$ state in its β decay to ^{215}Po and the much lower population of the $5/2^+$ state [26]. Therefore, based on the available literature data we fixed the spin of $^{217,219}\text{At}^g$ as $I = (9/2)$.

As shown in the complementary paper [27], the most probable spin of ^{218}At is $I = (3^-)$. The latter is based on the unhindered nature of the ^{218}At α decay populating presumably the $E = 63\,\text{keV}$, $I = (3^-)$ excited state in ^{214}Bi. However, the $I^{\pi} = (2^-)$ assignment cannot be completely ruled out (see Ref. [27] for details). In the present study, due to the Doppler-limited resolution, it was also impossible to choose between the fit results with $I = 2$ or 3 assignments [see Figs. 1(b) and 1(c)]. Thus, for $^{218}\text{At}^g$, both spin options, $I(^{218}\text{At}^g) = (2, 3)$, must be considered.

B. Extraction of nuclear parameters

The data were analyzed with a fixed hfs a-constant ratio, $\rho \equiv a(58805\,\text{cm}^{-1})/a(46234\,\text{cm}^{-1}) = -1.69(2)$ [19]. The hyperfine constants and isotope shifts for ^{217,218,219}At are presented in Table I.

The magnetic dipole moments, μ_A, were calculated using the scaling relation with ^{211}At as a reference:

$$\mu_A = \mu_{\text{ref}} \frac{a_A(46234\text{cm}^{-1})I_A}{a_{\text{ref}}(46234\text{cm}^{-1})I_{\text{ref}}}. \tag{1}$$

The following reference values were used: $a_{211}(46234\,\text{cm}^{-1}) = -367(4)\,\text{MHz}$, $\mu_{211} = 4.139(37)\mu_N$ [19]. A possible hyperfine structure anomaly (HFA) was taken into account by increasing the uncertainty: by 1% for ^{218}At with $I \neq 9/2$ and by 0.1% for $^{217,219}\text{At}(I = 9/2)$ (see detailed discussion in Ref. [19] and compilation of the available HFA data in Ref. [28]).

To deduce the electric quadrupole moment Q_S from the measured hfs b constant, the ratio b/Q_S was calculated for the astatine atomic ground state by applying the multiconfiguration Dirac-Hartree-Fock (MCDHF) method [19]. The full description of numerical methods can be found in Ref. [29]. With the measured ratio of the b constants for the atomic ground state and the excited state at $46234\,\text{cm}^{-1}$ [19], one obtains: $b(46234\,\text{cm}^{-1})/Q_S = 600(300)\,\text{MHz/b}$. The main

TABLE II. Magnetic dipole and electric quadrupole moments, changes in mean-square charge radii, and staggering parameter γ_A (see below) for ^{217,218,219}At. For ^{218}At, the results for the different possible spin assignments (see Sec. III A) are presented. Statistical and systematic uncertainties are given in round and curly brackets, respectively. The systematic uncertainties in $\delta\langle r^2 \rangle_{A,205}$, stem from the theoretical indeterminacy of the F and M factors; in μ, from the uncertainty in μ_{ref} and the HFA indeterminacy; and in Q_S, from the uncertainty in the theoretical b/Q_S ratio.

Atomic number	I	$\mu(\mu_N)$	$Q_S(b)$	$\delta\langle r^2 \rangle_{A,205}(\text{fm}^2)$	γ_A
217	(9/2)	3.703(45) {56}	−1.40(25) {70}	1.194(7) {62}	
218	(2)	1.195(84) {29}	0.63(33) {32}	1.369(11) {71}	1.45(11)
218	(3)	1.25(12) {3}	0.55(33) {27}	1.349(11) {70}	1.29(11)
219	(9/2)	3.502(45) {53}	−1.17(25) {59}	1.435(10) {74}	

contribution to the uncertainty stems from the error in the b-constants ratio.

The changes in the mean-square charge radii, $\delta\langle r^2 \rangle_{A,A'}$, were deduced from the measured isotope shift $\delta\nu_{A,A'}$ using the relations:

$$\delta\nu_{A,A'} = \delta\nu_{A,A'}^F + \delta\nu_{A,A'}^M,$$
$$\delta\nu_{A,A'}^F = F\delta\langle r^2 \rangle_{A,A'}, \qquad (2)$$
$$\delta\nu_{A,A'}^M = \frac{M(A - A')}{AA'},$$

where $\delta\nu_{A,A'}^F$ and $\delta\nu_{A,A'}^M$ are the field and mass shifts, respectively, F is an electronic factor, $M = M^{\text{NMS}} + M^{\text{SMS}}$, and M^{NMS} and M^{SMS} are the normal mass shift (NMS) and specific mass shift (SMS) constants, respectively. The electronic factors, F and M^{SMS}, were determined for the 795-nm transition by MCDHF calculations: $F(\text{At}; 795\,\text{nm}) = -11.47(57)\,\text{GHz fm}^{-2}$, $M^{\text{SMS}}(\text{At}; 795\,\text{nm}) = -580(100)$ GHz amu [19]. In this case a different approach to considering electron correlations in comparison with the MCDHF calculations of the b/Q_S ratio was implemented (see details in Refs. [19,30]).

The magnetic dipole moments, electric quadrupole moments, and changes in the mean-square charge radii for ^{217,218,219}At are presented in Table II. The magnetic moment of ^{217}At was measured previously by the low temperature nuclear orientation method [31]: $\mu(^{217}\text{At}) = 3.81(18)\mu_N$. Our result (see Table II) agrees with the literature value in the limits of uncertainties.

IV. MAGNETIC AND QUADRUPOLE MOMENTS

A. *g* factors for even-*N* isotopes

In Fig. 2 the g factors ($g = \mu/I$) for the odd-Z, even-N nuclei with $N \geqslant 126$ are presented. Along with the results of the present work for $_{85}$At isotopes, the data for $_{83}$Bi ([32] and references therein), $_{87}$Fr ([33,34]), and $_{89}$Ac [35,36] isotopes are shown. Horizontal dotted lines mark the single-particle values of the g factors near doubly magic ^{208}Pb, for the relevant proton orbitals: $\pi i_{13/2}$ [37], $\pi f_{7/2}$ [38], and $\pi h_{9/2}$ (Schmidt estimation). All experimental g factors shown in Fig. 2 lie between the Schmidt value for the $\pi h_{9/2}$ orbital and the g factor for the 9/2$^-$ ground state of semimagic ^{209}Bi. This suggests that the leading configuration for all of these nuclei

is $\pi h_{9/2}$, despite the change in spin from 9/2 to 5/2 in ^{221}Fr and 3/2 in ^{223,225}Fr and ^{227}Ac.

As is seen in Fig. 2, the g factors for different Z decrease at similar rate with increasing N, although there is a jump for Fr isotopes at $N = 136$ when the spin changes from 5/2 to 3/2. After this jump, the gradual decrease in the g factor with respect to N is restored, with the same rate of change as for the $N = 126-132$ isotopes of francium with $I = 9/2$. This jump may be explained by an admixture from a $\pi f_{7/2}$ configuration, which has a larger single-particle g factor (see Fig. 2). Indeed, the $I^\pi = 3/2^-$ ground state of ^{223}Fr is presumed to have a deformed $3/2^-$[521]$f_{7/2}$ Nilsson configuration, which is strongly mixed with the $1/2^-$[521]$h_{9/2}$ band [39].

Although the g factors for the odd astatine isotopes studied in the present work also decrease when going from $N = 132$ to $N = 134$ at the same rate as for the isotonic francium isotopes, its absolute value is markedly larger than that for ^{219,221}Fr$_{132,134}$ (see Fig. 2). This increase may be attributed to the admixture of other higher-j proton configurations. It cannot be explained by the spherical $f_{7/2}-$ configuration
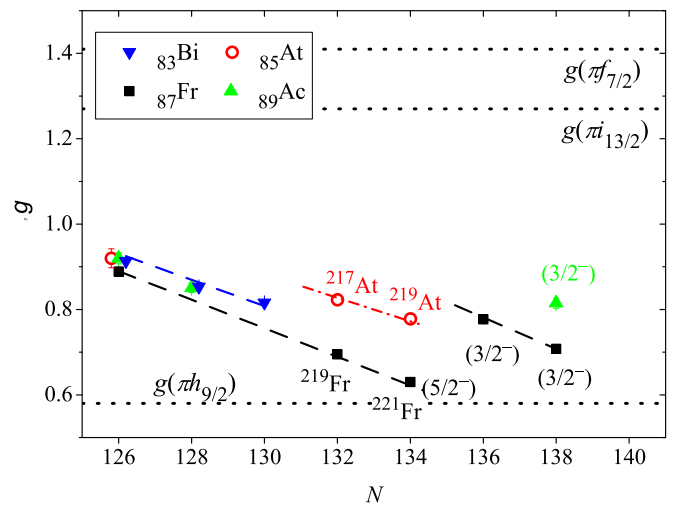

FIG. 2. g factors for the even-N, $N \geqslant 126$ isotopes of astatine (open circles), francium (squares), actinium (upward triangles), and bismuth (downward triangles). The data points without labels in parentheses correspond to the nuclei with $I^\pi = 9/2^-$, whereas the spins for other isotopes are explicitly shown. Lines of the same slope connecting the points for different isotopes are shown.

admixture, due to the lower spin in this configuration. However, if one assumes the presence of octupole deformation, then mixing between opposite-parity orbitals stemming from $\pi = -1 \, h_{9/2}$ and $\pi = +1 \, i_{13/2}$ configurations becomes possible and the admixture of the $i_{13/2}$ configuration would result in an increase of the magnetic moment $[g(i_{13/2}) > g(h_{9/2})$, $g(i_{13/2}) > g(9/2^-, {}^{209}\text{Bi})]$. Thus, the deviation of $g({}^{217,219}\text{At})$ from the systematics may be connected with the appearance of octupole collectivity in these nuclei.

B. *g* factor for odd-*N* isotope

Comparisons of the experimental magnetic moment of odd-odd nuclei, with estimations from the additivity relation, μ_{add}, [40] may aid in understanding nucleon orbital occupations. The most probable configuration for ${}^{218}\text{At}$ is $(\pi 1 h_{9/2} \otimes \nu 2 g_{9/2})_{2^-,3^-}$. For the additivity-rule calculations, individual empirical g factors for the $\pi 1 h_{9/2}$ and $\nu 2 g_{9/2}$ orbitals were taken from the magnetic moments of the closest odd-*A* isotopes available: $\mu_p = \mu({}^{217}\text{At}) = 3.7(1)\mu_N$ (present work), $\mu_n = \mu({}^{217}\text{Po}) = -1.11(14)\mu_N$ [15]. The results from the additivity-relation calculation are systematically lower than the experimental data for both possible spin assignments: $\mu_{\text{add}}({}^{218}\text{At}; 2^-) = 0.58(6)\mu_N$, $\mu_{\text{exp}}({}^{218}\text{At}; 2^-) = 1.20(11)\mu_N$ and $\mu_{\text{add}}({}^{218}\text{At}; 3^-) = 0.87(9)\mu_N$, $\mu_{\text{exp}}({}^{218}\text{At}; 3^-) = 1.25(12)\mu_N$. This may point to a possible admixture from other orbitals. Closely lying orbitals that could contribute to this admixture are $\pi f_{7/2}$ or $\pi i_{13/2}$ for the odd proton, and $\nu h_{11/2}$ for the odd neutron. However, for every two-particle combination of these orbitals other than that involving $i_{13/2}$ proton, the calculated μ_{add} value is lower than that of a $(\pi 1 h_{9/2} \otimes 2 g_{9/2})_{2^-,3^-}$ configuration. In the case of the configurations with $i_{13/2}$ proton, μ_{add} becomes significantly larger (μ_{add} for 2^+ or 3^+ states with the $i_{13/2}$ proton is in the region of $4-7\mu_N$, depending on the neutron state), thus, even a small admixture from these configurations would ensure an agreement between the additivity-rule estimations and the experimental results. Such an admixture is only possible in cases with mixing between opposite-parity states at nonzero octupole deformation. It is worth to note that the configuration mixing in ${}^{217,218,219}\text{At}$ with taking into account also the possible neutron excitations, may be probed by the large-scale shell-model calculations. Unfortunately, at present for astatine isotopes only the calculations with the limited number of the valence neutrons are available ($A < 216$; [41]).

C. Quadrupole moments

The quadrupole moments of the $9/2^-$ ground states in ${}^{217,219}\text{At}$ measured in the present work, indicate a small oblate deformation ($\beta_2 \approx -0.08$), in the strong coupling scheme (see Ref. [19] and references therein on the applicability of this approach for weakly deformed nuclei).

It is instructive to compare the ${}^{217,219}\text{At}$ results with ${}^{219}\text{Fr}$. The measured Q_S values for ${}^{217,219}\text{At}_{132,134}$ (see Table II) match within the limit of uncertainties with $Q_S({}^{219}\text{Fr}_{132}) = -1.21(2)\,\text{b}$ [34]. However, there is a difference in the understanding of the nature of the astatine and francium ground

states. The $9/2^-$ ground state in ${}^{219}\text{Fr}$ was proposed to be an anomalous member of the $K = 1/2^-$ band (K is the projection of the intrinsic spin on the symmetry axis), based on the $1/2^-[521]h_{9/2}$ orbital at a moderate prolate deformation [42]. The odd-proton spin is decoupled from the nuclear deformation axis in this nucleus, yielding a negative quadrupole moment at a positive deformation (see Ref. [34] and references therein). In contrast, the $K = 1/2^-$ band was not observed in ${}^{217,219}\text{At}$. The $9/2^-$ ground states in these nuclei are considered to be spherical $h_{9/2}$ states or $9/2^-[505]h_{9/2}$ states with small oblate deformation (see Ref. [43] and references therein). Surprisingly, despite such an obvious difference in the interpretation of the $9/2^-$ ground states in the isotonic francium and astatine nuclei, the corresponding quadrupole moments have nearly the same values.

Similar to the use of the additivity rule for magnetic moments, spectroscopic quadrupole moments for odd-odd nuclei can be estimated by applying a single-particle quadrupole additivity rule based on a general tensor coupling scheme (see Refs. [44,45] and references therein). Deviations from this quadrupole additivity rule may be attributed to the development of collectivity. We applied this additivity rule to ${}^{218}\text{At}$ with the following single-particle quadrupole moments: $Q_{S,p} = Q_S({}^{217}\text{At})$ (present work) and $Q_{S,n} = Q_S({}^{217}\text{Po})$ [15]. The resulting values of $Q_{S,\text{add}}({}^{218}\text{At}; I = 3) = 0.41(27)\,\text{b}$, $Q_{S,\text{add}}({}^{218}\text{At}; I = 2) = 0.45(29)\,\text{b}$ agree within the limits of uncertainties with the experimental values: $Q_{S,\text{exp}}({}^{218}\text{At}; I = 3) = 0.55(33)\,\text{b}$, $Q_{S,\text{exp}}({}^{218}\text{At}; I = 2) = 0.63(33)\,\text{b}$. However, in view of the large experimental uncertainties, no definite conclusion on the level of collectivity can be drawn from the present data.

To summarize, the analysis of the magnetic dipole and electric quadrupole moments of the ${}^{217,218,219}\text{At}$ isotopes shows that these nuclei are satisfactorily described within the framework of the spherical shell model. However, there are some indications for the possible presence of the octupole collectivity, which will be further emphasized by the discussion of the charge radii, presented in the next section.

V. CHANGES IN MEAN-SQUARE CHARGE RADII

A. Shell effect

In Fig. 3, changes in the mean-square charge radii $\delta\langle r^2 \rangle$ for the astatine nuclei near $N = 126$ are shown (for $N \leqslant 126$ the values from Ref. [19] are used), along with the droplet-model (DM) predictions [46]. As is seen in Table II, the radii obtained for ${}^{218}\text{At}$ with different spin assumptions, coincide within the experimental uncertainties and would be indistinguishable in Fig. 3, therefore only the $\delta\langle r^2 \rangle_{218 \,(I=3),\, 211}$ value is presented.

A characteristic increase in the slope of the $\delta\langle r^2 \rangle$ isotopic dependency when crossing the neutron magic number $N = 126$ is evident (although the IS for ${}^{212-216}\text{At}$ was not measured due to their short half lives). This shell effect in radii was found to be a universal feature of the $\delta\langle r^2 \rangle$ behavior and was observed for different isotopic chains near $N = 28, 50, 82, 126$ [47].
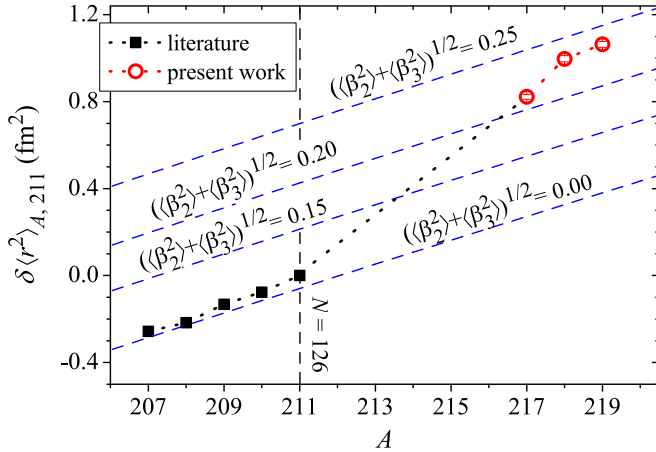
FIG. 3. Changes in the mean-square charge radii for astatine isotopes near the shell closure at $N = 126$. Open circles: present work; squares: Ref. [19]. The experimental points are connected by a dotted line to guide the eye. The dashed lines show the droplet model predictions with constant deformation.

FIG. 4. Shell-effect parameters for the lead-region nuclei. Filled squares: parameter ξ_{even}, hollow squares: parameter ξ_{even}^*. The experimental points for ξ_{even}^* are connected by dotted line to guide the eye. Triangles show the results of the RMF calculations with DD-PC1 energy-density functional.

To compare the shell effect in different isotopic chains, the dimensionless shell-effect parameter, ξ_{even}, was used [32]:

$$\xi_{\text{even}} \equiv \frac{\delta \langle r^2 \rangle_{128,126}}{\delta \langle r^2 \rangle_{126,124}} = \frac{\delta \nu^F_{128,126}}{\delta \nu^F_{126,124}}, \qquad (3)$$

where the subscript indices are the neutron numbers. This parameter is independent of the uncertainties in the F factor (usually 5–10% in the lead region; note that in the case of astatine the uncertainty in ξ_{even} due to the M-factor indeterminacy is less than 0.5%). The choice of the even-N isotopes with $N = 124, 128$, being the nearest to the neutron magic number $N = 126$, helps to avoid mixing of the shell effect with other effects which might contribute to the observed $\delta \langle r^2 \rangle$ value. However, when there are no experimental data for $N = 128$ nuclei, it is instructive to assume linear interpolation and consider also the modified shell-effect parameter which takes into account heavier nuclei with known $\delta \langle r^2 \rangle$,

$$\xi_{\text{even}}^* \equiv \frac{2}{N_0 - 126} \frac{\delta \langle r^2 \rangle_{N_0, 126}}{\delta \langle r^2 \rangle_{126, 124}} = \frac{2}{N_0 - 126} \frac{\delta \nu^F_{N_0, 126}}{\delta \nu^F_{126, 124}}, \qquad (4)$$

where N_0 is the lowest even neutron number at $N > 126$ with measured IS: $N_0 = 132$ for $_{84}$Po [48,49], $_{85}$At (present work), $_{86}$Rn [6,50], $_{87}$Fr [16,33,51], $_{88}$Ra [52], and $N_0 = 138$ for $_{89}$Ac [53]. For $_{82}$Pb and $_{83}$Bi isotopes, data for nuclei with $N = 124, 126, 128$ were taken from Refs. [54] and [32], respectively.

In Fig. 4 the shell-effect parameters for lead-region nuclei are presented and compared with the results of relativistic mean-field (RMF) calculations with DD-PC1 energy-density functional [55]. It should be reminded that the standard nonrelativistic Hartree-Fock (NRHF) approach fails to explain this effect [ξ_{even}(NRHF)] ~ 1 [56,57]. A detailed discussion on the different theoretical descriptions of the shell-effect, as well as the analysis of the shell effect for odd-N nuclei can be found in Ref. [32].
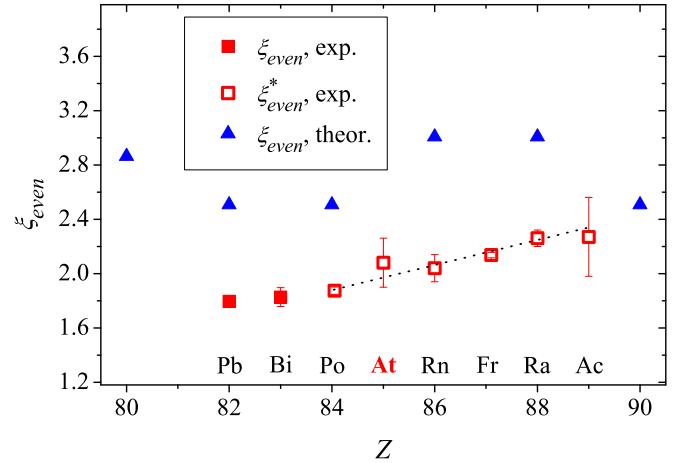
Theoretical RMF calculations overestimate ξ_{even}. A better description of the shell effect for lead nuclei was recently obtained with a new extended parameterization of the RMF model based on the effective field theory (see Fig. 2 in Ref. [58]), in the relativistic Hartree-Fock approach with nonlinear terms and density-dependent meson-nucleon coupling [59], and in the Hartree-Fock-Bogoliubov calculations using a density-dependent spin-orbit interaction [60].

The parameter ξ_{even}^* linearly increases with Z (by $\sim$20% when going from $Z = 84$ to $Z = 89$). It is unclear whether this trend is due to a Z dependence of the shell-effect, or it is connected with the different deformation contribution to $\delta \langle r^2 \rangle_{N_0, 126}$ at different Z (through $\delta \langle \beta_2^2 \rangle$ and $\delta \langle \beta_3^2 \rangle$), or it is a result of the linear interpolation used in the extraction of the modified shell parameter.

B. Odd-even staggering

The odd-even staggering in nuclear charge radii is quantified by the staggering parameter, introduced by Tomlinson and Stroke [61] (for odd N),

$$\gamma_N = \frac{2\delta \langle r^2 \rangle_{N-1, N}}{\delta \langle r^2 \rangle_{N-1, N+1}} = \frac{2\delta \nu^F_{N-1, N}}{\delta \nu^F_{N-1, N+1}}. \qquad (5)$$

When $\gamma_N = 1$, there is no OES, whereas $\gamma < 1$ and $\gamma > 1$ correspond to normal and inverse OES, respectively. The γ parameter does not depend on the electronic factor and its uncertainty; therefore it is well suited to compare quantitatively the OES for the different isotopic chains.

The γ values for the isotopes of $_{85}$At (present work, [19]), $_{82}$Pb [54], $_{84}$Po [24,48,49,62], $_{87}$Fr [16,34,51], $_{88}$Ra [52], and $_{86}$Rn [6,50] are plotted as a function of neutron number in Fig. 5. The OES parameters for $_{83}$Bi$_{123,125,127}$ [32] coincide within the limits of uncertainties with that of the isotonic $_{82}$Pb isotopes and are excluded from the plot for clarity. The values of γ_{123} and γ_{125} for $_{88}$Ra and $_{86}$Rn isotopes also coincide with those for the isotonic nuclei and are also excluded.
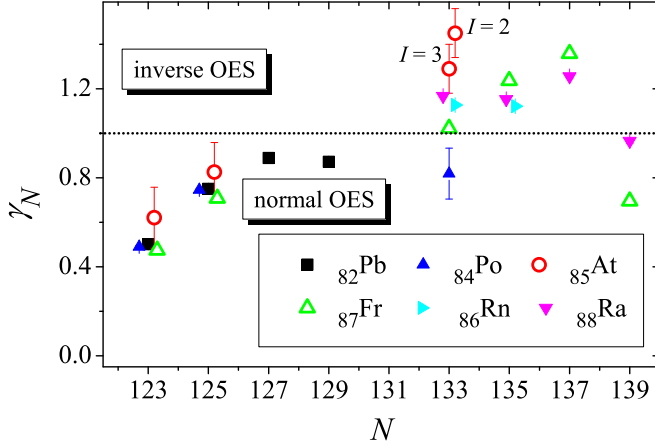
FIG. 5. Values of the odd-even staggering parameter, γ, for the different isotopic chains in the lead region near the $N = 126$ shell closure: $_{82}$Pb (squares), $_{84}$Po (filled upward triangles), $_{85}$At (hollow circles), $_{86}$Rn (rightward triangles), $_{87}$Fr (hollow upward triangles), and $_{88}$Ra (downward triangles). For ^{218}At the γ values determined with the assumptions $I(^{218}\text{At}) = 2$ and $I(^{218}\text{At}) = 3$, are both shown. The dotted horizontal line represents the absence of the OES, $\gamma_N = 1$.

As is seen in Fig. 5, the OES at $N < 131$ and at $N > 137$ is normal for all isotopic chains ($\gamma_N < 1$), whereas for $_{87}$Fr, $_{88}$Ra, and $_{86}$Rn isotopes with $133 \leqslant N \leqslant 137$, $\gamma_N > 1$, which means the inverted OES effect. Our new data for $^{217-219}$At testify to the retention of this effect for $Z = 85$. As described in Sec. I, there is a strong correlation between inverse OES and octupole deformation. Correspondingly, one can suppose the possible presence of octupole collectivity in astatine nuclei near $N = 133$.

This assumption is quite surprising, since the region of quadrupole-octupole deformation is supposedly confined between $Z = 86$ and $Z = 92$ (see Table I in Ref. [63]). Moreover, so far no evidence for parity doublet bands and their associated fast $E1$ transitions has been observed in ^{217,219}At [43], the appearance of which is usually regarded as a signature of octupole collectivity. In contrast with the isotonic francium isotopes where such signs of the octupole collectivity are firmly established [42], low-lying states in ^{217,219}At can be reliably described as parts of the seniority-three proton configurations: $(h_{9/2})^3$ and $(h_{9/2})^2 f_{7/2}$, that is, as spherical shell-model states without invoking octupole or quadrupole deformation [42]. Unfortunately, the data on the excited states in ^{218}At are missing. Thus, it is unknown whether the parity doublet bands and the other signs of octupole collectivity are present in this nucleus.

In contrast with the majority of the presumed octupole deformed nuclei [63], spins of ^{217,218,219}At are reasonably well described by the spherical shell-model $\pi h_{9/2}$ and $\pi h_{9/2} \otimes \nu g_{9/2}$ configurations (see Sec. IV A). Thus, so far firm nuclear spectroscopic evidence for quadrupole-octupole deformation in ^{217,218,219}At has not been observed (see also Ref. [64]) and inverse OES remains the single definite experimental indication on the possible octupole deformation in these nuclei.

However, potential-energy surface (PES) calculations, in the framework of the macroscopic-microscopic approach, also testify to the presence of the quadrupole-octupole deformed minimum in the PES for $^{217-219}$At [65]. This minimum is supposed to correspond to the ground state since it is deeper by 0.5–0.6 MeV than the minimum in the PES calculated with the assumption of zero octupole deformation [65].

Using the results of these calculations, we deduced the theoretical value of the OES parameter, $\gamma_{133,\text{theor}}$, for the At isotopes via the relation [6]

$$\langle r^2 \rangle = \langle r^2 \rangle_{\text{DM}} \left[1 + \frac{5}{4\pi} \left(\langle \beta_2^2 \rangle + \langle \beta_3^2 \rangle + \langle \beta_4^2 \rangle \right) \right], \qquad (6)$$

where $\langle r^2 \rangle_{\text{DM}}$ is a mean-square charge radius calculated by the droplet model [46] and β_λ is a deformation parameter. The β_λ values were derived from the ε_λ parameters presented in Ref. [65], using the corresponding relations [66]. The result, $\gamma_{133,\text{theor}}(\text{At}) = 1.3$, agrees well with the experimental value [$\gamma_{133,\text{exp}}(\text{At}; 3^-) = 1.29(11)$; $\gamma_{133,\text{exp}}(\text{At}; 2^-) = 1.45(11)$]. It is worth noting that similar calculations for Fr isotopes give $\gamma_{133,\text{theor}}(\text{Fr}) = 1.1$, and are also in agreement with experiment [$\gamma_{133,\text{exp}}(\text{Fr}) = 1.02(11)$].

To summarize, keeping in mind the OES systematics for nuclei with $N \geqslant 132$, we believe that the observed large inverse OES in heavy isotopes of astatine is related to the presence of octupole collectivity, either for all three investigated isotopes (^{217,218,219}At), or only for odd-odd ^{218}At. This assumption is supported by the PES calculations. However, further nuclear spectroscopic information is required in order to substantiate this inference.

VI. CONCLUSIONS

Hyperfine structure parameters and isotope shifts have been measured for ^{217,218,219}At, using the 795-nm atomic transitions. Magnetic dipole and electric quadrupole moments, and changes in the nuclear mean-square charge radii have been deduced and discussed in the framework of the possible presence of octupole collectivity.

Analysis of the electromagnetic moments shows that ^{217,218,219}At are reasonably well described within the framework of the spherical shell model. However, the discrepancy between the additivity-rule prediction and experimental data for $\mu(^{218}\text{At})$ may qualitatively indicate the presence of the quadrupole-octupole collectivity.

The shell effect in the mean-square charge radii of the astatine isotopes when crossing $N = 126$ has been observed. The increase of the shell-effect parameter with Z may also be related to the increase in quadrupole-octupole collectivity at $N = 132$, when going from $Z = 84$ to $Z = 88$.

A large inverse odd-even staggering in radii has been found for ^{217,218,219}At. This result is surprising since for the isotonic $_{87}$Fr isotopes the OES disappears, and the $_{85}$At isotopes are expected to lie outside the region of the quadrupole-octupole collectivity, where inverse OES was previously established. The assumption of the presence of the quadrupole-octupole collectivity in heavy astatine isotopes is supported by the potential-energy surface calculations, although so far there

is no nuclear-spectroscopic evidence from the excited states which could substantiate this inference.

ACKNOWLEDGMENTS

[1] P. A. Butler and W. Nazarewicz, Rev. Mod. Phys. **68**, 349 (1996).

[2] P. A. Butler, J. Phys. G: Nucl. Part. Phys. **43**, 073002 (2016).

[3] F. S. Stephens, Jr., F. Asaro, and I. Perlman, Phys. Rev. **100**, 1543 (1955).

[4] L. P. Gaffney *et al.*, Nature **497**, 199 (2013).

[5] P. Möller, R. Bengtsson, B. G. Carlsson, P. Olivius, and T. Ichikawa, Phys. Rev. Lett. **97**, 162502 (2006).

[6] E. W. Otten, in *Treatise on Heavy-Ion Science*, edited by D. A. Bromley (Plenum, New York, 1989), Vol. 8, p. 517.

[7] G. A. Leander and R. K. Sheline, Nucl. Phys. A **413**, 375 (1984).

[8] I. Talmi, Nucl. Phys. A **423**, 189 (1984).

[9] D. Nosek, R. K. Sheline, P. C. Sood, and J. Kvasil, Z. Phys. A **344**, 277 (1993).

[10] R. K. Sheline, A. K. Jain, and K. Jain, Phys. Rev. C **38**, 2952 (1988).

[11] G. D. Alkhazov *et al.*, Z. Phys. A **337**, 257 (1990).

[12] K. Dörschel *et al.*, Z. Phys. A **317**, 233 (1984).

[13] R. K. Sheline, Phys. Lett. B **219**, 222 (1989).

[14] F. Buchinger, J. E. Crawford, A. K. Dutta, J. M. Pearson, and F. Tondeur, Phys. Rev. C **49**, 1402 (1994).

[15] D. A. Fink *et al.*, Phys. Rev. X **5**, 011018 (2015).

[16] I. Budinčević *et al.*, Phys. Rev. C **90**, 014317 (2014).

[17] K. M. Lynch *et al.*, Phys. Rev. C **97**, 024309 (2018).

[18] V. L. Truesdale *et al.*, Phys. Rev. C **94**, 034308 (2016).

[19] J. Cubiss *et al.*, Phys. Rev. C **97**, 054327 (2018).

[20] G. D. Alkhazov *et al.*, Nucl. Instrum. Methods Phys. Res., Sect. B **69**, 517 (1992).

[21] B. A. Marsh *et al.*, Nucl. Instrum. Methods Phys. Res., Sect. B **317**, 550 (2013).

[22] H. De Witte *et al.* Phys. Rev. Lett. **98**, 112502 (2007).

[23] R. N. Wolf *et al.*, Int. J. Mass Spectrom. **349**, 123 (2013).

[24] M. D. Seliverstov *et al.*, Phys. Rev. C **89**, 034323 (2014).

[25] M. S. Basunia, Nucl. Data Sheets **108**, 633 (2007).

[26] B. Singh, G. Mukherjee, D. Abriola, S. K. Basu, P. Demetriou, A. Jain, S. Kumar, S. Singh, and J. Tuli, Nucl. Data Sheets **114**, 2023 (2013).

[27] J. Cubiss *et al.*, Phys. Rev. C (to be published).

[28] J. R. Persson, At. Data Nucl. Data Tables **99**, 62 (2013).

[29] J. Bieroń, C. Froese Fischer, S. Fritzsche, G. Gaigalas, I. P. Grant, P. Indelicato, P. Jönsson, and P. Pyykkö, Phys. Scr. **90**, 054011 (2015), and references therein.

[30] E. Eliav, S. Fritzsche, and U. Kaldor, Nucl. Phys. A **944**, 518 (2015), and references therein.

[31] M. Lindroos, P. Richards, J. Rikovska, N. J. Stone, I. Oliveira, K. Nishimura, M. Booth, and the NICOLE and ISOLDE Collaborations, Hyperfine Interact. **75**, 323 (1992).

[32] A. E. Barzakh, D. V. Fedorov, V. S. Ivanov, P. L. Molkanov, F. V. Moroz, S. Yu. Orlov, V. N. Panteleev, M. D. Seliverstov, and Yu. M. Volkov, Phys. Rev. C **97**, 014322 (2018), and references therein.

[33] A. Coc *et al.*, Phys. Lett. **163B**, 66 (1985).

[34] R. P. de Groote *et al.*, Phys. Rev. Lett. **115**, 132501 (2015).

[35] D. Decman *et al.*, Nucl. Phys. A **436**, 311 (1985).

[36] C. Granados *et al.*, Phys. Rev. C **96**, 054331 (2017).

[37] T. Yamazaki, T. Nomura, S. Nagamiya, and T. Katou, Phys. Rev. Lett. **25**, 547 (1970).

[38] A. E. Stuchbery, A. P. Byrne, and G. D. Dracoulis, Nucl. Phys. A **555**, 369 (1993).

[39] R. K. Sheline, C. F. Liang, P. Paris, J. Kvasil, and D. Nosek, Phys. Rev. C **51**, 1708 (1995).

[40] R. J. Blin-Stoyle, Rev. Mod. Phys. **28**, 75 (1956).

[41] K. Yanase, E. Teruya, K. Higashiyama, and N. Yoshinaga, Phys. Rev. C **98**, 014308 (2018).

[42] C. F. Liang, P. Paris, J. Kvasil, and R. K. Sheline, Phys. Rev. C **44**, 676 (1991), and references therein.

[43] C. F. Liang, P. Paris, and R. K. Sheline, Phys. Rev. C **64**, 034310 (2001).

[44] J. Eberz *et al.*, Z. Phys. A **326**, 121 (1987).

[45] G. Neyens, Rep. Prog. Phys. **66**, 633 (2003).

[46] D. Berdichevsky and F. Tondeur, Z. Phys. A: At. Nucl. **322**, 141 (1985).

[47] I. Angeli, Yu. P. Gangrsky, K. P. Marinova, I. N. Boboshin, S. Yu. Komarov, B. S. Ishkhanov, and V. V. Varlamov, J. Phys. G: Nucl. Part. Phys. **36**, 085102 (2009).

[48] D. Kowalewska, K. Bekk, S. Göring, A. Hanser, W. Kalber, G. Meisel, and H. Rebel, Phys. Rev. A **44**, R1442 (1991).

[49] T. E. Cocolios *et al.*, Phys. Rev. Lett. **106**, 052503 (2011).

[50] W. Borchers *et al.*, Hyperfine Interact. **34**, 25 (1987).

[51] V. A. Dzuba, W. R. Johnson, and M. S. Safronova, Phys. Rev. A **72**, 022503 (2005).

[52] L. W. Wansbeek, S. Schlesser, B. K. Sahoo, A. E. L. Dieperink, C. J. G. Onderwater, and R. G. E. Timmermans, Phys. Rev. C **86**, 015503 (2012).

[53] R. Ferrer *et al.*, Nat. Commun. **8**, 14520 (2017).

[54] M. Anselment, W. Faubel, S. Göring, A. Hanser, G. Meisel, H. Rebel, and G. Schatz, Nucl. Phys. A **451**, 471 (1986).

[55] S. E. Agbemava, A. V. Afanasjev, D. Ray, and P. Ring, Phys. Rev. C **89**, 054320 (2014); see Supplemental Material at http://link.aps.org/supplemental/10.1103/PhysRevC.89.054320.

[56] M. M. Sharma, G. A. Lalazissis, and P. Ring, Phys. Lett. B **317**, 9 (1993).

[57] N. Tajima, P. Bonche, H. Flocard, P.-H. Heenen, and M. S. Weiss, Nucl. Phys. A **551**, 434 (1993).

[58] B. Kumar, S. K. Singh, B. K. Agrawal, and S. K. Patra, Nucl. Phys. A **966**, 197 (2017).

[59] W. Long, J. Meng, N. Van Giai, and S.-G. Zhou, Phys. Rev. C **69**, 034319 (2004).

[60] H. Nakada and T. Inakura, Phys. Rev. C **91**, 021302(R) (2015).

[61] W. J. Tomlinson and H. H. Stroke, Nucl. Phys. **60**, 614 (1964).

[62] M. D. Seliverstov *et al.*, Phys. Lett. B **719**, 362 (2013).

[63] R. K. Sheline, Phys. Lett. B **197**, 500 (1987).

[64] R. K. Sheline, C. F. Liang, and P. Paris, Phys. Rev. C **51**, 1192 (1995).

[65] P. Möller, R. Bengtsson, B. G. Carlsson, P. Olivius, T. Ichikawa, H. Sagawa, and A. Iwamoto, At. Data Nucl. Data Tables **94**, 758 (2008).

[66] G. A. Leander and Y. S. Chen, Phys. Rev. C **37**, 2744 (1988).